

# Compression of Exact Wavefunctions with Restricted Boltzmann Machine Auto-Encoders

Anderson D. S. Duraes\*

*Department of Chemistry and Biochemistry, University of Notre Dame,  
251 Nieuwland Science Hall, Notre Dame, IN 46556, USA*

(Dated: July 2018)

Virtually, every ab-initio electronic structure method (Coupled Cluster, DMRG, etc.) can be viewed as an algorithm to compress the ground-state wavefunction. This compression is usually obtained by exploiting some physical structure of the wavefunction, which leads to issues when the system changes and that structure is lost. Compressions which are efficient near equilibrium (coupled cluster) or in 1-D systems (DMRG) often fail catastrophically elsewhere. To overcome these issues, we seek a scheme that compresses wavefunctions without any supervised physical information. In this manuscript, we introduce a scheme to compress molecular wavefunctions using a model for high dimensional functions from machine learning: a restricted Boltzmann machine (RBM). We show that, while maintaining chemical accuracy, the RBM can significantly compress the exact wavefunction.

## INTRODUCTION

In his Nobel lecture, Kohn stressed the problem of storing an accurate many-body wavefunction ( $\Phi$ ) for a large system on a classical computer. [1] For simple and direct model chemistries, like the full configuration interaction (FCI) method, the storage problem is essentially the main stumbling block to exact improvable results. [2–8] The FCI method employs a linear combination of all the possible Slater determinants ( $\Psi_n$ 's) in order to span the exact wavefunction ( $\Phi_{\text{FCI}}$ ): [2, 6–8]

$$\Phi_{\text{FCI}} = \sum_{n=0} c_n \Psi_n. \quad (1)$$

However, depending on the quantity of electrons and atomic orbitals of a system, the full set of electronic  $\Psi_n$ 's—and, consequently, the number of bits—are simply too numerous to manipulate on a classical machine; forbidding any FCI calculation for even modestly sized molecules. [2, 4, 6, 8, 9]

In order to face this storage problem, many authors have tried to compress  $\Phi_{\text{FCI}}$ . [2, 9–38] These compression algorithms are usually based on physical insights into the structure of the exact wavefunction or based on mathematical insights into approximate solutions of the ground state problem. These compressions exploit the fact that only a small fraction of the  $\Psi_n$ 's (Eq. 1) usually contribute to an accurate ground state wavefunction. [39, 40]

For instance, the selected CI plus perturbation theory correction (SCI+PT) algorithms [21–27]—such as the Heat-Bath CI (HBCI) [25]—implement deterministic constraints to select configuration expansions which significantly contribute to an accurate ground-state energy. Alternatively, Monte Carlo algorithms [28–38]—such as the FCI Quantum Monte Carlo (FCIQMC) [28–30]—implement stochastic constraints to select configuration expansions. Both methods are able to treat larger CI spaces than a naive approach. On the other hand,

these [deterministic/stochastic] constraints are somewhat arbitrary, generating a systematic source of error for the estimated FCI calculations. [17, 41]

We are instead curious about compressing the Slater determinants without any specific physical or mathematical structure, using a neural network to achieve a non-linear map. To do this, we apply the Restricted Boltzmann Machine (RBM).

RBM [42–49] is classified as an unsupervised learning algorithm and its structure consists of two layers: one layer having the visible units and the other, the binary hidden units. [42–48] The visible units process the input data, and the hidden units designs the compression of the input. [42–48] The bridge between the two layers—visible units to hidden units—is established by parameters that connect both units in a process denominated as encoding. [42–48, 50, 51] The reverse process, known as decoding, uses the binary hidden units—with the same parameters in the encoding—to recover the uncompressed (original) input data. [42–48, 50, 51]

In addition, RBM has found successful application to compress images [52–55], to model data [43, 56–60], and even to study physical systems [49, 61–69]. Besides, connections between RBM and tensor networks have been recently reported. [70, 71]

In this paper, we apply the RBM method to compress the Slater determinants of the FCI ground-state wavefunctions of four singlet molecules:  $\text{BeH}_2$ ,  $\text{C}_2$ ,  $\text{N}_2$ , and  $\text{F}_2$ . On top of that, we investigate the reduction of the configuration spaces induced by the RBM, and generate potential energy surfaces (PES's) within a chemical accuracy level (1 kcal/mol). By the results, the RBM method sounds to be an alternative approach of lessening the computational cost of the determinant-based CI algorithms.

### Encoding Process

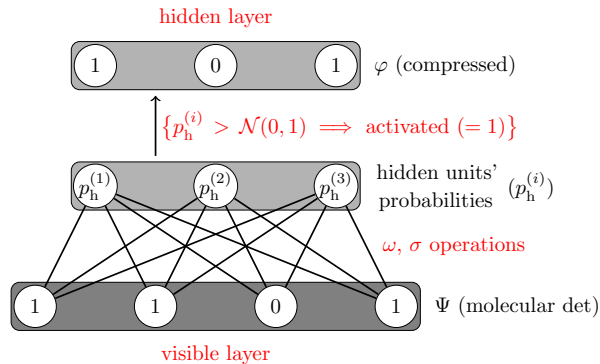


FIG. 1. Encoding Process: a fictitious molecular determinant (det), [1,1,0,1], which has 4 bits, is compressed to [1,0,1], which has 3 bits.  $\omega$  is a set of weights that connect the visible and hidden layers,  $\sigma$  is a logistic function,  $\mathcal{N}(0,1)$  is a normal distribution with mean 0 and variance 1, and “ $\Rightarrow$ ” is the “implies” symbol. The molecular determinants denote the [occupied (=1) / virtual (=0)] spin atomic orbitals of a given system. See [Formalism](#) for details. [72]

### FORMALISM

Our task is to find a compact representation of the Slater configurations ( $\Psi_n$ 's) that span  $\Phi_{\text{FCI}}$  (Eq. 1). Each  $\Psi_n$ 's is binary, since the configurations represent the occupied (= 1) and virtual (= 0) spin atomic orbitals [6–8]. Being the number of spin atomic orbitals predefined by the basis set of the atoms that compose a system. [6,8]

Suppose “ $i$ ” is a unit of the hidden layer (h) and “ $j$ ” is a unit of the visible layer (v). Let  $\varphi$  be the compressed configuration associated to  $\Psi$  (a member of the  $\Psi_n$ 's), and  $\omega$ , a set of weights which connects the visible and the hidden layer.

The encoding process (FIG. 1.) can be expressed by  $p_h^{(i)}$ , the probability of the hidden unit “ $i$ ”: [42–48,50,51]

$$p_h^{(i)} = \sigma \left\{ d_i + \sum_j [\Psi]_j \omega_{ji} \right\}, \quad (2)$$

where  $\sigma(t) = 1/[1 + \exp(-t)]$  (a logistic function),  $d_i$  is a bias parameter, and the sum runs over all the “ $j$ ” units of  $\Psi$ .

If  $p_h^{(i)}$  is greater than a random number coming from a normal distribution with mean 0 and variance 1, then the hidden unit “ $i$ ” is activated (“ $i$ ” = 1). [44,46] Otherwise, it is not activated (“ $i$ ” = 0). As a result of this stochastic process,  $\varphi$  is binary like  $\Psi$ .

Analogously, the decoding process (FIG. 2.) can be expressed by  $p_v^{(j)}$ , the probability of the reconstructed unit “ $j$ ”: [42–48,50,51]

### Decoding Process

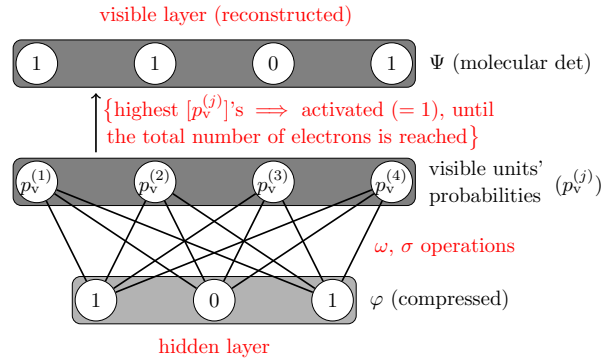


FIG. 2. Decoding Process: starting from the compressed representation, [1,0,1], the same fictitious molecular determinant (det) from Figure 1 is reconstructed. The symbols are defined in Figure 1 and in [Formalism](#). Observe the distinctiveness between  $p_v^{(j)}$  and  $p_h^{(i)}$  [in FIG. 1.] to, respectively, reconstruct and compress the molecular det. Because the number of electrons is held constant, the reconstructed determinant will certainly belong to the studied system. [72]

$$p_v^{(j)} = \sigma \left\{ e_j + \sum_i [\varphi]_i \omega_{ij} \right\}, \quad (3)$$

where  $e_j$  is a bias parameter and the sum runs over all the “ $i$ ” units of  $\varphi$ .

On the other hand, the activation of the reconstructed visible units goes in another way. To ensure that the reconstructed configurations belong to a given system, the units with the highest  $[p_v^{(j)}]$ 's become 1—until the total number of electrons of the given system is reached—and then the remaining units become zero.

From the formalism above, it is important to note that a reconstructed determinant can be generated from more than one different compressed representation. Nevertheless, a compressed representation can recover only one of the original molecular determinants.

For the next Sections, since the input configurations are molecular determinants, we name this kind of RBM as “molecular RBM”.

### COMPUTATIONAL DETAILS

STO-3G [73–75] is the basis set for the four singlet systems studied here: BeH<sub>2</sub>, C<sub>2</sub>, N<sub>2</sub>, and F<sub>2</sub>. All the electronic structure calculations are performed on PySCF package [76], adopting the Löwdin-orthogonalized orbitals [7,77]. And, for each system, a molecular RBM is trained by the single-step contrastive divergence algorithm [44,46,78] on a slightly modified version of the

Chen *et al.*'s code [46]—at the present time, the training is evaluated by the sum of the squared FCI coefficients of not repeated reconstructed configurations, and the units of the reconstructed configurations obey the total number of electrons of a given system to be activated (*vide Formalism*).

Turning to the training set, it follows the alpha and beta string introduced by Handy [8, 79–81], in a manner to guarantee that the determinants are eigenfunctions of  $\hat{S}_Z$  (the z-component of the spin operator) [6, 8, 82–84]. Besides, for each system, the training set is composed of the necessary molecular determinants to recover the ground-state FCI electronic energy—within a chemical accuracy level—of 30 dissociation geometries. These geometries have varying distance (R), ranging from 0.3 to 3.2 angstrom (Å), equally spaced by 0.1 Å.

For all the systems, the dissociation of the molecules into their atoms takes place in one dimension; with a particular attention to the hydrogens in BeH<sub>2</sub>. Both hydrogens are dissociated from the Be atom in an equal fashion. Or, in other words, for each geometry in BeH<sub>2</sub>, the distance H-Be—which ranges from 0.3 to 3.2 Å in the training set—is identical for the other H atom.

After the molecular RBM is trained, each one of all the  $n$ th-excited configurations, from the analyzed molecule, is sampled 100 times through the encoding and decoding processes. The decoding process' output with the highest frequency is pointed out as the reconstructed determinant, and the associated encoding output is pointed out as the compressed representation. In the end, the ground-state electronic energy for the molecular RBM is calculated by a projection of the reconstructed determinants onto the FCI determinants, using the Davidson diagonalization method [76, 85, 86].

In this work, the spatial symmetries of the four molecules are not explored.

## ASSESSING THE COMPRESSION

The amount of bits per molecular determinant is associated to the number of occupied and virtual atomic orbitals for the uncompressed configurations, and to the number of hidden units for the compressed ones.

With this, we consider the following metric to evaluate the compression achieved by the molecular RBM.

$$\text{TNB} = \sum_s \text{fbits}(\mathcal{Y}_s), \quad (4)$$

where “TNB” = Total Number of Bits, “fbits” is a function which counts the number of bits of the  $s$ th compressed/not compressed molecular determinant ( $\mathcal{Y}_s$ ). And the sum runs through not repeated configurations.

Physically, this metric concatenates all the determinants of a system in the same line and computes the num-

TABLE I. Comparing the space savings and the nonparallelism error (NPE) for the molecular RBM (mRBM) and the spin-adapted (SA) CCSD(RHF), under the four singlet systems. [89]

Systems	BeH <sub>2</sub>	C <sub>2</sub>	N <sub>2</sub>	F <sub>2</sub>
<b>Total number of bits (TNB)<sup>a</sup></b>				
FCI	17,150	882,000	288,000	2,000
SA CCSD(RHF)	1,274	6,500	5,060	1,100
mRBM	3,260	737,064	52,845	406
<b>Space savings<sup>b</sup> (%)</b>				
SA CCSD(RHF)	92.6	99.3	98.2	45.0
mRBM	81.0	16.4	81.7	79.7
<b>NPE<sup>a, c</sup> (kcal/mol)</b>				
CCSD(RHF)	4.94	38.3	144.4	0.0
mRBM	0.0	0.1	0.3	0.3

<sup>a</sup> (See [Assessing the Compression](#) for definition.)

<sup>b</sup> Space savings =  $\{1 - \text{TNB}(\text{compressed})/\text{TNB}(\text{FCI})\}$

<sup>c</sup> For the interval  $R \in [0.3, 5.8]$  Å.

ber of bits of this concatenation. Furthermore, the metric above not only consider the compression for each configuration in the CI expansion, but also considers the reduction of the configuration space that span  $\Phi_{\text{FCI}}$  (Eq. 1).

Since the studied systems are singlet, only configurations satisfying  $\langle \hat{S}_Z \rangle = 0$  (the expectation value of the  $\hat{S}_Z$  operator) [6, 8, 82–84] enter in the metric. Moreover, for the compressed configurations, TNB considers only the minimum compressed representations that recover not repeated uncompressed ones.

Moving to the PES, we consider the nonparallelism error (NPE) [87, 88] to evaluate the potential curve generated by the compression. Within an interval R, NPE is defined by the distance between two points: the greatest and the lowest signed deviations compared to the FCI curve. [87, 88] And, for each considered molecule, NPE is calculated for the interval  $R \in [0.3, 5.8]$  Å.

## RESULTS AND DISCUSSION

In this section, we abbreviate “molecular RBM” to mRBM in tables and graphs. Besides, a comparison with CCSD(RHF) is established. CCSD stands for “coupled cluster singles (S) and doubles (D)”, adopting the Restricted Hartree-Fock (RHF) as the reference determinant for the singly and doubly-excited configurations. The number of bits for CCSD(RHF) is considered under the spin-adapted (SA) configurations [6, 8, 82], which is abbreviated as SA CCSD(RHF). SA configurations indicates that each configuration is not only an eigenfunction of  $\hat{S}_Z$ —like the uncompressed determinants considered here (see [Computational Details](#))—but also an eigenfunction of  $\hat{S}^2$  (the total spin-squared operator) [6, 8, 82–

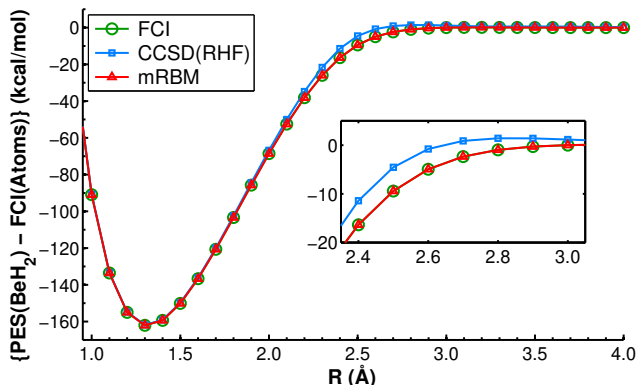


FIG. 3. PES for  $\text{BeH}_2$ , subtracting the ground-state FCI electronic energy of one Be and two H atoms from the three curves. (See text for details.)

84].

The unity for energy is kcal/mol and specific aspects of the calculations are in [Computational Details](#). In addition, under the STO-3G basis set,  $\text{F}_2$  has only up to doubly-excited configurations, and then CCSD(RHF) becomes exact like FCI.

Turning to Table I, it shows the total number of bits (TNB), the space savings, and the nonparallelism error (NPE) for PES—where the distance ( $R$ ) between atoms are in the interval  $[0.3, 5.8]$  Å.

TNB is linked to the space savings through the total number of bits of FCI: mRBM and SA CCSD(RHF) are the compression methods, and are compared to the uncompressed one (FCI). The space savings for mRBM are in the order of 80% for  $\text{BeH}_2$ ,  $\text{N}_2$  and  $\text{F}_2$ ; but it is 16.4% for  $\text{C}_2$ . On the other hand, the space savings for SA CCSD(RHF) exhibit values of the order of 95% for  $\text{BeH}_2$ ,  $\text{C}_2$  and  $\text{N}_2$ ; but it is 45.0% for  $\text{F}_2$ , when CCSD(RHF) is exact, *i.e.*, for SA CCSD(RHF), the space savings for the singlet  $\text{F}_2$  molecule relies just

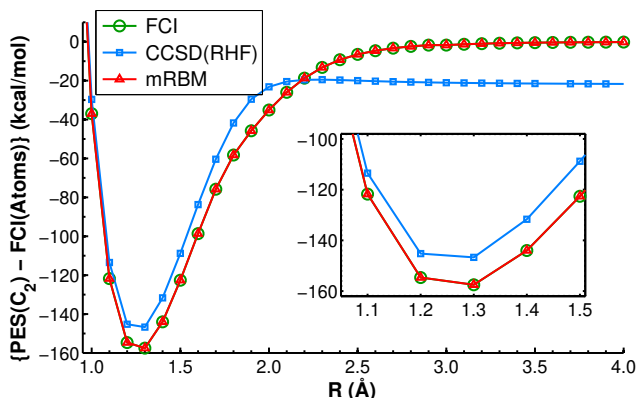


FIG. 4. PES for  $\text{C}_2$ , subtracting the ground-state FCI electronic energy of two C atoms from the three curves. (See text for details.)

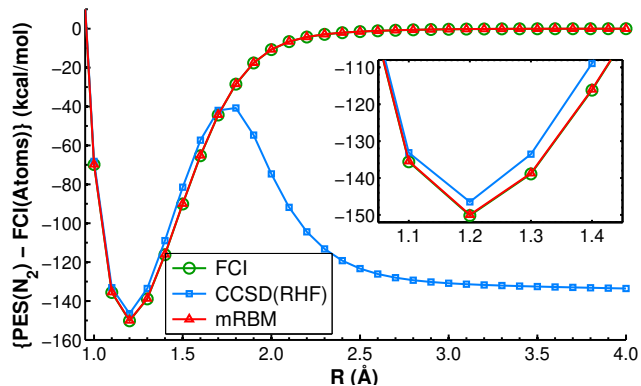


FIG. 5. PES for  $\text{N}_2$ , subtracting the ground-state FCI electronic energy of two N atoms from the three curves. (See text for details.)

on the SA configurations embraced.

However, the space savings *per se* does not tell much about how good a compression is, and therefore it must be combined with NPE and PES. Having this in mind, Figure 3 through 6 display PES's for the four singlet molecules, employing FCI, CCSD(RHF) and mRBM. In each PES, these three curves are subtracted by a constant—the ground-state FCI electronic energy for the atoms that compose a given molecule [ $\text{PES}(\text{molecule}) - \text{FCI}(\text{Atoms})$ ].

For  $\text{BeH}_2$ , Figure 3 shows that CCSD(RHF) diverges from the FCI curve from  $R = 1.9$  to  $R = 3.2$  Å, and it is reflected by  $\text{BeH}_2$ 's NPE value of 4.94 kcal/mol (Table I). The molecular RBM, however, fully recovers the FCI curve, showing a NPE value of 0.0 kcal/mol.

In Figure 4, the CCSD(RHF) curve for  $\text{C}_2$  is qualitatively correct until  $R = 2.0$  Å. After that point, CCSD(RHF) predicts a lower dissociation energy, characterizing a large NPE value of 38.3 kcal/mol for this system. In its turn, mRBM overlaps FCI, with a lower

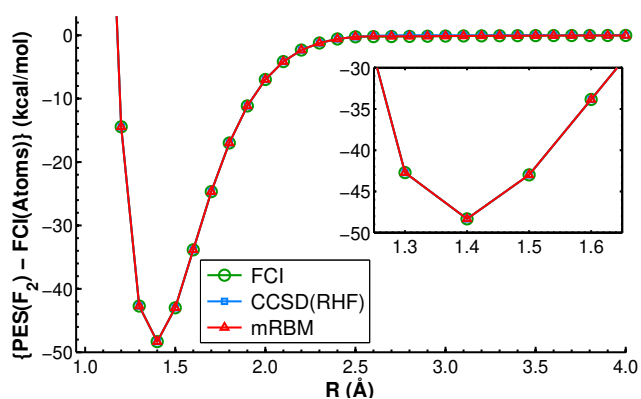


FIG. 6. PES for  $\text{F}_2$ , subtracting the ground-state FCI electronic energy of two F atoms from the three curves. (See text for details.)

NPE value of 0.3 kcal/mol. Similarly, Figure 5 reveals that the CCSD(RHF) curve for  $N_2$  is qualitatively correct until  $R = 1.7 \text{ \AA}$ . And, thereafter, it predicts an incorrect dissociation energy. The NPE value for this CCSD(RHF) curve is the largest one in Table I: 144.4 kcal/mol. Considering the mRBM, it practically overlaps the FCI curve, exhibiting a lower NPE value of 0.3 kcal/mol.

The dissociation problem faced by CCSD(RHF), in Figures 4 and 5, is known as the size-consistency issue. Due to the RHF reference configuration adopted, this coupled cluster method is not size-consistent in principle. [83,90,91]

The last figure—Figure 6—displays the PES for  $F_2$ . As pointed out before, CCSD(RHF) is exact for this molecule, implying a zero value for NPE. The molecular RBM curve basically lies over FCI as well, but with a NPE value of 0.3 kcal/mol.

In summary, after combining the space savings and NPE from Table I, and the four PES's in Figures 3–6; the higher compression of CCSD(RHF)—credited for only considering singly and doubly-excited configurations—come at a price: its PES's for  $BeH_2$ ,  $C_2$ , and  $N_2$  are not chemical accurate. In contrast, the molecular RBM shows large space savings for  $BeH_2$ ,  $N_2$ , and  $F_2$ , and it generates PES's that are chemical accurate for all the four studied molecules.

## CONCLUSION

The molecular RBM not only compresses the molecular determinants, but also truncates the FCI expansion. Because of these facts, mRBM is a possible way of decreasing the computational cost of determinant-driven CI algorithms. Each mRBM includes configurations that are essential for the analyzed system, within a chemical accuracy level, generating smooth PES and providing space savings that are comparable to the CCSD(RHF) method.

Different than the coupled cluster, and as a kind of truncated CI expansion, mRBM satisfy the variational theorem [6–8,81,84], and therefore predicts ground-state energies which are upper bounds of the exact ones.

Lastly, an atomic version of the RBM—as building blocks for molecules—could increase the compression already achieved by mRBM; and could be a universal approximation to efficiently truncate the FCI expansion for any system over any geometry. These concepts are under investigation and will be compared to the mRBM in the near future.

---

\* anderson.duraes@nd.edu

[1] W. Kohn, *Rev. Mod. Phys.* **71**, 1253 (1999).

[2] J. Bauschlicher, Charles W., S. R. Langhoff, and P. R. Taylor, *Accurate Quantum Chemical Calculations*, Tech.

Rep. NASA-TM-101932 (NASA Ames Research Center, 1989).

[3] B. Roos, *Chem. Phys. Lett.* **15**, 153 (1972).

[4] J. Olsen, P. Jørgensen, and J. Simons, *Chem. Phys. Lett.* **169**, 463 (1990).

[5] R. Shepard, *J. Comput. Chem.* **11**, 45 (1990).

[6] A. Szabo and N. S. Ostlund, *Modern Quantum Chemistry: Introduction to Advanced Electronic Structure Theory*, Dover Books on Chemistry (Dover Publications, Mineola, New York, 1996).

[7] I. Mayer, *Simple Theorems, Proofs, and Derivations in Quantum Chemistry*, Mathematical and Computational Chemistry (Springer US, Boston, MA, 2003).

[8] T. Helgaker, P. Jørgensen, and J. Olsen, *Molecular Electronic-Structure Theory* (John Wiley & Sons, Ltd, 2000).

[9] P. R. Taylor, *J. Chem. Phys.* **139**, 074113 (2013).

[10] J. R. McClean and A. Aspuru-Guzik, *RSC Adv.* **5**, 102277 (2015).

[11] P. J. Knowles, *Mol. Phys.* **113**, 13 (2015).

[12] K. H. Marti, B. Bauer, M. Reiher, M. Troyer, and F. Verstraete, *New J. Phys.* **12**, 103008 (2010).

[13] R. J. Buenker and S. D. Peyerimhoff, *Theor. Chim. Acta* **35**, 33 (1974).

[14] T. Zhang and F. A. Evangelista, *J. Chem. Theory Comput.* **12**, 4326 (2016).

[15] L. Bytautas and K. Ruedenberg, *J. Chem. Phys.* **121**, 10905 (2004).

[16] L. Bytautas and K. Ruedenberg, *J. Chem. Phys.* **122**, 154110 (2005).

[17] P. M. Zimmerman, *J. Chem. Phys.* **146**, 104102 (2017).

[18] L. Bytautas, T. M. Henderson, C. A. Jiménez-Hoyos, J. K. Ellis, and G. E. Scuseria, *J. Chem. Phys.* **135**, 044119 (2011).

[19] D. R. Alcoba, A. Torre, L. Lain, O. B. Oña, P. Capuzzi, M. V. Raemdonck, P. Bultinck, and D. V. Neck, *J. Chem. Phys.* **141**, 244118 (2014).

[20] D. R. Alcoba, A. Torre, L. Lain, G. E. Massaccesi, O. B. Oña, P. W. Ayers, M. V. Raemdonck, P. Bultinck, and D. V. Neck, *Theor. Chem. Acc.* **135**, 153 (2016).

[21] B. Huron, J. P. Malrieu, and P. Rancurel, *J. Chem. Phys.* **58**, 5745 (1973).

[22] S. Evangelisti, J.-P. Daudey, and J.-P. Malrieu, *Chem. Phys.* **75**, 91 (1983).

[23] R. J. Harrison, *J. Chem. Phys.* **94**, 5021 (1991).

[24] R. Roth, *Phys. Rev. C* **79**, 064324 (2009).

[25] A. A. Holmes, N. M. Tubman, and C. J. Umrigar, *J. Chem. Theory Comput.* **12**, 3674 (2016).

[26] N. M. Tubman, J. Lee, T. Y. Takeshita, M. Head-Gordon, and K. B. Whaley, *J. Chem. Phys.* **145**, 044112 (2016).

[27] J. B. Schriber and F. A. Evangelista, *J. Chem. Phys.* **144**, 161106 (2016).

[28] G. H. Booth, A. J. W. Thom, and A. Alavi, *J. Chem. Phys.* **131**, 054106 (2009).

[29] D. Cleland, G. H. Booth, and A. Alavi, *J. Chem. Phys.* **132**, 041103 (2010).

[30] G. H. Booth, S. D. Smart, and A. Alavi, *Mol. Phys.* **112**, 1855 (2014).

[31] F. R. Petruzielo, A. A. Holmes, H. J. Changlani, M. P. Nightingale, and C. J. Umrigar, *Phys. Rev. Lett.* **109**, 230201 (2012).

[32] S. Ten-no, *J. Chem. Phys.* **138**, 164126 (2013).

[33] J. C. Greer, *J. Chem. Phys.* **103**, 1821 (1995).

- [34] L. Tong, M. Nolan, T. Cheng, and J. Greer, *Comput. Phys. Commun.* **131**, 142 (2000).
- [35] J. P. Coe and M. J. Paterson, *J. Chem. Phys.* **137**, 204108 (2012).
- [36] T. P. Kelly, A. Perera, R. J. Bartlett, and J. C. Greer, *J. Chem. Phys.* **140**, 084114 (2014).
- [37] A. A. Holmes, H. J. Changlani, and C. J. Umrigar, *J. Chem. Theory Comput.* **12**, 1561 (2016).
- [38] Y. Ohtsuka and J.-Y. Hasegawa, *J. Chem. Phys.* **147**, 034102 (2017).
- [39] J. Ivanic and K. Ruedenberg, *Theor. Chem. Acc.* **106**, 339 (2001).
- [40] L. Bytautas and K. Ruedenberg, *Chem. Phys.* **356**, 64 (2009).
- [41] R. J. Azar and M. Head-Gordon, *J. Chem. Phys.* **142**, 204101 (2015).
- [42] P. Smolensky, “Information processing in dynamical systems: Foundations of harmony theory,” in *Parallel Distributed Processing: Explorations in the Microstructure of Cognition, Vol. 1: Foundations*, edited by D. E. Rumelhart, J. L. McClelland, and C. PDP Research Group (MIT Press, Cambridge, MA, USA, 1986) pp. 194–281.
- [43] Y. Freund and D. Haussler, “Unsupervised learning of distributions on binary vectors using two layer networks,” in *Advances in Neural Information Processing Systems 4*, edited by J. E. Moody, S. J. Hanson, and R. P. Lippmann (Morgan-Kaufmann, 1992) pp. 912–919.
- [44] G. E. Hinton, “A Practical Guide to Training Restricted Boltzmann Machines,” in *Neural Networks: Tricks of the Trade: Second Edition*, edited by G. Montavon, G. B. Orr, and K.-R. Müller (Springer Berlin Heidelberg, Berlin, Heidelberg, 2012) pp. 599–619.
- [45] G. E. Hinton, S. Osindero, and Y.-W. Teh, *Neural Comput.* **18**, 1527 (2006).
- [46] E. Chen, M. Chandra, V. Shukela, and C. Connors, “Restricted boltzmann machines in python,” <https://github.com/echen/restricted-boltzmann-machines/blob/master/rbm.py> (2017).
- [47] N. Le Roux and Y. Bengio, *Neural Comput.* **20**, 1631 (2008).
- [48] G. Montufar and N. Ay, *Neural Comput.* **23**, 1306 (2011).
- [49] G. Carleo and M. Troyer, *Science* **355**, 602 (2017).
- [50] Y. Bengio, “Practical Recommendations for Gradient-Based Training of Deep Architectures,” in *Neural Networks: Tricks of the Trade: Second Edition*, edited by G. Montavon, G. B. Orr, and K.-R. Müller (Springer Berlin Heidelberg, Berlin, Heidelberg, 2012) pp. 437–478.
- [51] D. P. Kingma and M. Welling, (2013), [arXiv:1312.6114](https://arxiv.org/abs/1312.6114).
- [52] G. E. Hinton and R. R. Salakhutdinov, *Science* **313**, 504 (2006).
- [53] A. Torralba, R. Fergus, and Y. Weiss, “Small Codes and Large Image Databases for Recognition,” in *2008 IEEE Conf. Comput. Vis. Pattern Recognit.* (IEEE, 2008) pp. 1–8.
- [54] C. Cheng, S. Wang, X. Chen, and Y. Yang, *Int. J. Distrib. Sens. Networks* **12**, 1851829 (2016).
- [55] V. Lokare, S. Birari, and O. Patil, *Int. J. Comput. Sci. Inf. Technol.* **6**, 4799 (2015).
- [56] R. Salakhutdinov, A. Mnih, and G. Hinton, “Restricted Boltzmann Machines for Collaborative Filtering,” in *Proc. 24th Int. Conf. Mach. Learn. - ICML '07* (ACM Press, New York, New York, USA, 2007) pp. 791–798.
- [57] H. Larochelle and Y. Bengio, “Classification using Discriminative Restricted Boltzmann Machines,” in *Proc. 25th Int. Conf. Mach. Learn. - ICML '08* (ACM Press, New York, New York, USA, 2008) pp. 536–543.
- [58] E. P. Xing, R. Yan, and A. G. Hauptmann, (2012), appears in Proceedings of the Twenty-First Conference on Uncertainty in Artificial Intelligence (UAI2005), [arXiv:1207.1423](https://arxiv.org/abs/1207.1423).
- [59] U. Fiore, F. Palmieri, A. Castiglione, and A. De Santis, *Neurocomputing* **122**, 13 (2013).
- [60] R. Salakhutdinov and G. Hinton, “Learning a Nonlinear Embedding by Preserving Class Neighbourhood Structure,” in *Proceedings of the Eleventh International Conference on Artificial Intelligence and Statistics*, Proceedings of Machine Learning Research, Vol. 2, edited by M. Meila and X. Shen (PMLR, San Juan, Puerto Rico, 2007) pp. 412–419.
- [61] Y. Nomura, A. S. Darmawan, Y. Yamaji, and M. Imada, *Phys. Rev. B* **96** (2017).
- [62] T. Lesieur, F. Krzakala, L. Zdeborová, M. Benedetti, J. Realpe-Gómez, A. Perdomo-Ortiz, A. Decelle, G. Fissore, and C. Furtlehner, *EPL* **119** (2017).
- [63] S. Weinstein, (2017), [arXiv:1707.03114](https://arxiv.org/abs/1707.03114).
- [64] K.-I. Aoki and T. Kobayashi, *Mod. Phys. Lett. B* **30**, 1650401 (2016).
- [65] L. Huang and L. Wang, *Phys. Rev. B* **95** (2017).
- [66] A. Decelle, G. Fissore, and C. Furtlehner, (2018), [arXiv:1803.01960](https://arxiv.org/abs/1803.01960).
- [67] D.-L. Deng, X. Li, and S. Das Sarma, *Phys. Rev. B* **96**, 195145 (2017).
- [68] J. Biamonte, P. Wittek, N. Pancotti, P. Rebentrost, N. Wiebe, and S. Lloyd, *Nature* **549**, 195 (2017).
- [69] D.-L. Deng, X. Li, and S. Das Sarma, *Phys. Rev. X* **7**, 021021 (2017).
- [70] J. Chen, S. Cheng, H. Xie, L. Wang, and T. Xiang, *Phys. Rev. B* **97** (2018).
- [71] Y. Huang and J. E. Moore, (2017), [arXiv:1701.06246](https://arxiv.org/abs/1701.06246).
- [72] This figure was constructed using TikZ, from a modified example at <https://github.com/MartinThoma/LaTeX-examples/tree/master/tikz>.
- [73] W. J. Hehre, R. F. Stewart, and J. A. Pople, *J. Chem. Phys.* **51**, 2657 (1969).
- [74] D. Feller, *J. Comput. Chem.* **17**, 1571 (1996).
- [75] K. L. Schuchardt, B. T. Didier, T. Elsethagen, L. Sun, V. Gurumoorthi, J. Chase, J. Li, and T. L. Windus, *J. Chem. Inf. Model.* **47**, 1045 (2007).
- [76] Q. Sun, T. C. Berkelbach, N. S. Blunt, G. H. Booth, S. Guo, Z. Li, J. Liu, J. D. McClain, E. R. Sayfutyarova, S. Sharma, S. Wouters, G. Kin, and L. Chan, (2017), [arXiv:1701.08223v2](https://arxiv.org/abs/1701.08223v2).
- [77] P. O. Löwdin, *J. Chem. Phys.* **18**, 365 (1950).
- [78] G. E. Hinton, *Neural Comput.* **14**, 1771 (2002).
- [79] N. Handy, *Chem. Phys. Lett.* **74**, 280 (1980).
- [80] P. Knowles and N. Handy, *Chem. Phys. Lett.* **111**, 315 (1984).
- [81] C. D. Sherrill and H. F. Schaefer, “The Configuration Interaction Method: Advances in Highly Correlated Approaches,” in *Advances in Quantum Chemistry*, Vol. 34, edited by P. O. Löwdin, J. R. Sabin, M. C. Zerner, and E. Brändas (Academic Press, 1999) pp. 143–269.
- [82] R. Pauncz, *Spin Eigenfunctions: Construction and Use* (Springer US, 1979).
- [83] B. O. Roos, *Lecture Notes in Quantum Chemistry II: European Summer School in Quantum Chemistry*, Vol. 64 (Springer-Verlag Berlin Heidelberg, 1994).

- [84] R. Shankar, *Principles of Quantum Mechanics* (Springer US, 1994).
- [85] E. R. Davidson, *J. Comput. Phys.* **17**, 87 (1975).
- [86] M. L. Leininger, C. D. Sherrill, W. D. Allen, and H. F. Schaefer, *J. Comput. Chem.* **22**, 1574 (2001).
- [87] X. Li and J. Paldus, *J. Chem. Phys.* **103**, 1024 (1995).
- [88] P. Josef and L. Xiangzhu, “A Critical Assessment of Coupled Cluster Method in Quantum Chemistry,” in *Advances in Chemical Physics* (John Wiley & Sons, Inc., 1999) pp. 1–175.
- [89] See Supplemental Material at [URL will be inserted by publisher] for additional information about the uncompressed/compressed molecular determinants.
- [90] M. Head-Gordon, *J. Phys. Chem.* **100**, 13213 (1996).
- [91] T. J. Lee and P. R. Taylor, *Int. J. Quantum Chem.* **36**, 199 (1989).

---

## Supplemental Material for “Compression of Exact Wavefunctions with Restricted Boltzmann Machine Auto-Encoders”

This supplemental material contains extra information about the uncompressed molecular configurations and the compressed ones.

Table S1 shows the number of bits per molecular configuration and the quantity of molecular configurations for FCI, mRBM and spin-adapted (SA) CCSD(RHF).

For FCI and SA CCSD(RHF), the number of bits per configuration is associated to the amount of atomic orbitals of a system. On the other hand, for mRBM, this same number corresponds to the amount of hidden units of the trained RBM.

In its turn, the amount of hidden units is connected to the size of the training set, or, in other words, the RBM needs more hidden units to reconstruct training sets that include more molecular determinants. This can be seen by the ascending order of the training set— $F_2 < BeH_2 < N_2 < C_2$ —which is equal as the ascending order of the bits per molecular determinants of the mRBM.

Moving to the number of molecular configurations, Table S1 exposes that SA CCSD(RHF) has few configurations when compared to FCI and mRBM for  $BeH_2$ ,  $C_2$  and  $N_2$ —since SA CCSD(RHF) only considers singly and doubly-excited singlet SA configurations. However, it is not the case for  $F_2$ , when CCSD(RHF) becomes exact.

For mRBM, the number of molecular configurations indicates that the molecular RBM recovers configurations which does not belong to the training set and also reduces the number of configurations which span the FCI wavefunction. This reduction of the configuration space is more pronounced for  $BeH_2$ ,  $N_2$  and  $F_2$ , and less pronounced for  $C_2$ .

TABLE S1. Bits per molecular configurations and number of configurations for FCI, spin-adapted (SA) CCSD(RHF) and the molecular RBM (mRBM). The basis set is STO-3G and the orbitals follow the Löwdin’s symmetric orthogonalization scheme.

Systems	BeH <sub>2</sub>	C <sub>2</sub>	N <sub>2</sub>	F <sub>2</sub>
<b>Bits per molecular configurations</b>				
FCI / SA CCSD(RHF)	14	20	20	20
mRBM	10	18	15	7
<b>Spin-adapted (SA) molecular configurations</b>				
(RHF + S + D)	91	325	253	55
<b>Molecular configurations with <math>\langle \hat{S}_z \rangle = 0</math></b>				
FCI	1,225	44,100	14,400	100
Training Set	212	6,688	1,880	48
mRBM	326	40,948	3,523	58

(See **Assessing the Compression Sec.** *in paper* for details).

Molecular configurations; RHF = Restricted Hartree–Fock reference, S = singly excited and D = doubly excited. (See **Results and Discussion Sec.** *in paper* for details).

$\langle \hat{S}_z \rangle$  is the expectation value of the  $\hat{S}_z$  operator [the z-component of the spin operator]. For mRBM,  $\langle \hat{S}_z \rangle$  is computed for the reconstructed configuration [decoding process].

---